Neuron, Vol. 21, 235–248, July, 1998, Copyright ©1998 by Cell Press

Constraining Ligand-Binding Site Stoichiometry Suggests that a Cyclic Nucleotide–Gated Channel Is Composed of Two Functional Dimers

David T. Liu,* Gareth R. Tibbs,† Pierre Paoletti,§ and Steven A. Siegelbaum†‡§‖
*Integrated Program in Cellular, Molecular, and Biophysical Studies
†Center for Neurobiology and Behavior
‡Department of Pharmacology
§Howard Hughes Medical Institute
Columbia University
New York, New York 10032

Summary

Cyclic nucleotide–gated ion channels are composed of four pore-forming subunits. Binding of cyclic nucleotide to a site in the intracellular carboxyl terminus of each subunit leads to channel activation. Since there are four subunits, four binding events are possible. In this study, we investigate the effects of individual binding events on activation by studying channels containing one, two, three, or four functional binding sites. The binding of a single ligand significantly increases opening, although four ligands are required for full activation. The data are inconsistent with models in which the four subunits activate in a single concerted step (Monod-Wyman-Changeux model) or in four independent steps (Hodgkin-Huxley model). Instead, the four subunits may associate and activate as two independent dimers.

Introduction

Ligand-gated and voltage-gated ion channels are multisubunit proteins whose activation depends on the binding of multiple ligands or movement of multiple voltage sensors. Such activation mechanisms serve to steepen the relation between stimulus intensity and response and thus help ensure efficient neuronal signaling (Jackson, 1989). However, it has been difficult to determine how each individual ligand binding event or voltage sensor movement contributes to channel activation. As a result, it is not known whether activation depends on independent gating reactions within the individual subunits of a channel, as first suggested by Hodgkin and Huxley (1952), or on a concerted, cooperative interaction among the subunits, as suggested by Monod et al. (1965).

These questions have been perhaps most readily explored for channels that can be formed as homomultimers, such as the tetrameric voltage-gated K channels (MacKinnon, 1991) and the related tetrameric cyclic nucleotide–gated (CNG) channels (Liu et al., 1996), involved in visual and olfactory signal transduction (see Finn et al., 1996; Zagotta and Siegelbaum, 1996, for reviews). Studies of the gating properties of heteromeric channels composed of both mutant and wild-type subunits have provided evidence for a cooperative interaction among subunits of both K channels (Tytgat and Hess, 1992; Schoppa et al., 1992; McCormack et al., 1994) and CNG channels (Goulding et al., 1994; Varnum and Zagotta, 1996). However, these studies could not measure the exact contribution of each subunit to channel gating, nor did they explicitly define the nature of the cooperative gating mechanism. Recently, Ruiz and Karpen (1997) addressed such questions by tethering variable numbers of light-activated cyclic GMP analogs to CNG channels. They concluded that successive ligand binding events caused a progressive increase in channel opening in a manner inconsistent with the Monod-Wyman-Changeux (MWC) model. However, since the authors had to rely on the gating properties of a channel to infer the number of attached ligands, the assignment of ligand stoichiometry may be open to other interpretations.

In this study, we have attempted to dissect directly the effects of each individual ligand binding step on CNG channel activation by constructing channels with constrained numbers of functional cyclic nucleotide–binding (CNB) sites. As each CNG channel subunit contains a 120-amino-acid cyclic nucleotide–binding domain in its carboxyl terminus that is homologous to CNB sites in other proteins (Kaupp et al., 1989; Shabb and Corbin, 1992; Tibbs et al., 1998), the tetrameric CNG channels contain four potential CNB sites. By coexpressing subunits with mutated binding sites with subunits possessing wild-type binding sites, we obtained heteromultimeric channels containing one, two, or three functional binding sites.

Our results show that the binding of even a single ligand causes a significant increase in channel open probability, although maximal channel opening requires the binding of all four ligands. The dependence of open probability on the number of bound ligands is inconsistent with either concerted (MWC) or independent (Hodgkin-Huxley) subunit models of gating. Instead, our data suggest that the tetrameric channel is composed of two functional dimers, each of which undergoes an independent transition between a resting and active state. Within each dimer, binding of ligands promotes entry into the active state, and the channel opens only after both dimers enter the active state.

Results

Use of Pore Conductance to Identify Subunit Stoichiometry

An important requirement for our experiments is to identify the subunit composition of heteromultimeric channels composed of subunits with wild-type CNB sites and subunits with mutant CNB sites. To accomplish this aim, we took advantage of results from a previous study in which we coexpressed the small conductance bovine retinal subunit 1 (RET) with a large conductance pore chimera subunit (RO133) (Goulding et al., 1993; Liu et

‖To whom correspondence should be addressed.

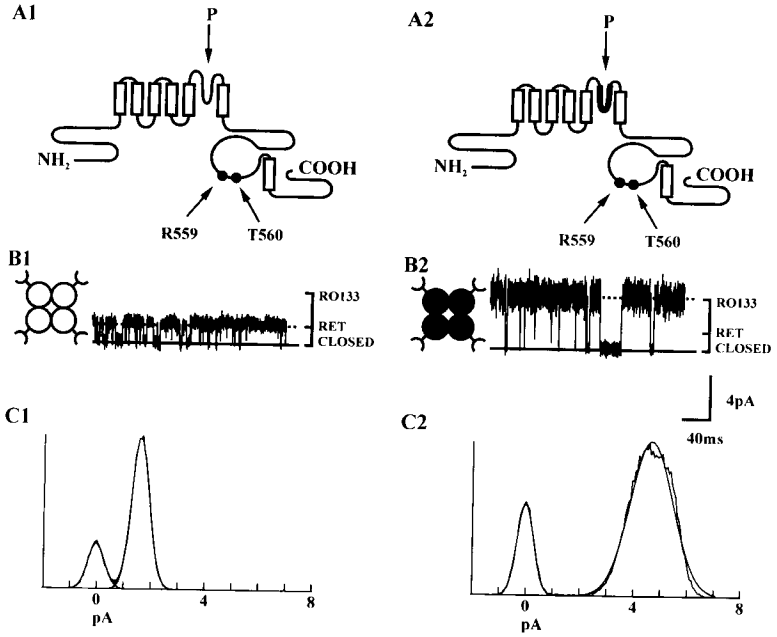

Figure 1. Schematic Representation of RET and RO133 Subunits and Representative Single-Channel Conductance Data of Homotetrameric RET and RO133 Channels

(A) Schematic representation of a single RET subunit (A1) and a single RO133 subunit (A2) indicating the pore-forming P loop (which lies between S5 and S6) and two key residues within the β roll of the carboxy-terminal cyclic nucleotide–binding domain, Arg-559 and Thr-560. In RO133, the P loop of RET has been replaced with the corresponding domain of the catfish olfactory channel (fOLF1, indicated by a thick line).

(B) Representative sweeps from patches containing either a single homomeric RET channel (B1) or a single homomeric RO133 channel (B2). In this and all subsequent figures, the deduced number and position of RET and RO133 subunits in a channel are shown schematically by the circle and sickle icons next to the traces. Each open circle represents a RET subunit; each closed circle represents an RO133 subunit. The sickle attached to each circle represents the CNB site of that subunit. Records obtained at +80 mV, pH 7.2.

(C) All-points amplitude histograms for the RET (C1) and RO133 (C2) channels shown in (B). Each of these distributions is well fitted with two Gaussian functions, representing the closed and open states of the channel. The conductances of the channels are 19 pS (RET) and 57 pS (RO133).

al., 1996). Coexpression of these two subunits yields four classes of intermediate conductance channels whose conductances provide a tag for subunit stoichiometry. The smallest intermediate conductance channel is comprised of one RO133 and three RET subunits, and the largest intermediate conductance channel contains one RET and three RO133 subunits. The two middle intermediate conductance channels each contain two RET and two RO133 subunits, but with distinct arrangements around the central pore (deduced from the properties of channels expressed from tandem dimers). Of the two, the channel with the smaller conductance has like subunits facing each other across the central pore (*trans* arrangement), and the channel with the larger conductance has like subunits adjacent to each other (*cis* arrangement).

In our original study, conductances were measured at an extracellular pH of 9.0 to decrease entry into proton-occupied subconductance states (Goulding et al., 1992; Root and MacKinnon, 1994). However, at pH 9.0, the lifetime of a patch recording tends to be short, making it difficult to obtain full dose response curves required in the present experiments. We therefore use here an external pH of 7.2 and measure channel conductance at +80 mV, a voltage that reduces (but does not eliminate) proton block. As shown in Figure 1, under these conditions homomeric RET channels display a conductance of around 20 pS (20.2 ± 0.5 pS, n = 5) whereas homomeric RO133 channels display a conductance of around 57 pS (57.3 ± 0.5, n = 6).

As from our earlier study (Liu et al., 1996), when RET and RO133 subunits are coexpressed and studied at pH 7.2 (+80 mV), we observe channels with intermediate conductance levels (Figures 2A1–2A4). Furthermore, a one-dimensional scatter plot of these data reveals that under these conditions, channel conductances also cluster around three intermediate levels (Figure 2D). These conductance levels occur at 27–30 pS, 36–40 pS, and 48–49 pS. Based on our previous results, we infer that these conductances represent channels composed of 1 RO133 and 3 RET subunits, 2 RO133 and 2 RET subunits (with subunits lying in either the *trans* or *cis* arrangement, although under these conditions, the difference in conductance between *cis* and *trans* is not as great as the difference observed at pH 9.0, −120 mV), and 1 RET and 3 RO133 subunits, respectively. We confirmed that the middle conductance cluster represents two RET and two RO133 subunits, in either the *trans* or *cis* arrangement, by using tandem dimer constructs (Figures 2B and 2C). Thus, expression of RET-RO133 heterodimers, in which like subunits are constrained to lie in the *trans* arrangement, yields 37 pS channels (37.4 ± 0.3, n = 2), whereas coexpression of RET-RET and RO133-RO133 homodimers, in which like subunits are constrained to lie in the *cis* arrangement, yields intermediate conductance channels of 40 pS (40.2 ± 0.2, n = 2). These conductances will be used below as tags for subunit stoichiometry.

Gating of Heteromultimeric Channels Containing One or More Mutant Binding Sites

To abolish binding of cyclic nucleotide to selected subunits, a key arginine in the CNB site that is conserved among all proteins with homologous cyclic nucleotide–binding domains (Shabb and Corbin, 1992; Tibbs et al., 1998) was mutated to a glutamate in RET (R559E), yielding the clone RET/E. We previously studied the effects of this mutation in the background of a chimeric channel, ROON-S2, which normally has a very high sensitivity to cGMP (Tibbs et al., 1998). In this background, the R559E mutation increased the $K_{1/2}$ (cGMP concentration producing half-maximal activation) by greater than 2000-fold but did not affect channel gating in response to

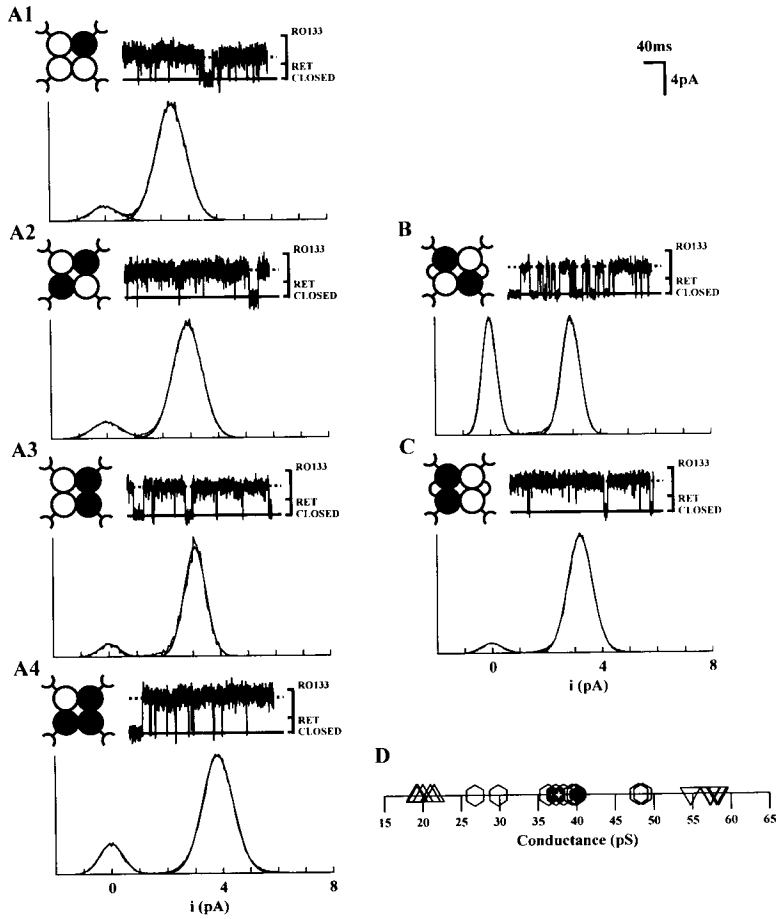

Figure 2. Coexpression of RET and RO133 Subunits Yields Channels that Have Intermediate Conductances

(A1–A4) Representative sweeps and all-points amplitude histograms obtained from four single-channel patches following coexpression of RET with RO133 subunit monomers. The subunit stoichiometry of each of these channels (see accompanying icons) was assigned on the basis of the conductances (30 pS, 36 pS, 40 pS, and 48 pS; [A1]–[A4], respectively) as determined from these histograms.

(B) Representative sweep and all-points amplitude histogram obtained from a single-channel patch following expression of the RO133-RET tandem heterodimer. Conductance is 37 pS.

(C) Representative sweep and all-points amplitude histogram obtained from a single-channel patch following coexpression of the RO133-RO133 tandem homodimer with the RET-RET tandem homodimer, yielding a channel with a 40 pS conductance.

(D) One-dimensional scatter plot of conductances for homotetrameric RET channels (open triangle, n = 5), homotetrameric RO133 channels (open inverted triangles, n = 6), and heteromultimeric channels with intermediate conductances upon coexpression of RET and RO133 monomer subunits (open hexagons, n = 9). Also plotted are intermediate conductance channels observed upon expression of RO133-RET tandem heterodimers (hexagons with plus sign, n = 2) and RO133-RO133 tandem homodimers with RET-RET tandem homodimers (closed hexagons, n = 2). All data were obtained at +80 mV, pH 7.2.

saturating cGMP (maximal open probability, P_{max}). An equivalent decrease in agonist affinity in the RET/E background should increase its $K_{1/2}$ from its normal value of 50–100 μM to greater than 100 mM. Consistent with the predicted effect of this mutation, we did not observe any cyclic nucleotide–activated channels when RET/E was expressed alone (using up to 30 mM cGMP).

However, when RET/E is coexpressed with RO133, functional channels at all expected intermediate conductances are observed (Figure 3). Moreover, channels with larger conductances (reflecting incorporation of a larger number of RO133 subunits and, hence, wild-type binding sites) are seen to have a higher open probability at a fixed ligand concentration. Thus, a channel with a conductance of 26 pS, comprised of three RET/E subunits and one RO133 subunit, has an open probability (P_O) of only 0.01 at 10 mM cGMP. Another channel with conductance of 42 pS (containing 2 RET/E and 2 RO133 subunits) has a P_O of 0.2, and two channels with conductances around 48 pS (composed of 1 RET/E and 3 RO133 subunits) have P_O values around 0.8. These data contrast with those obtained for RO133 homomultimers, which have a P_O of 0.95 (±0.02, n = 6; Tibbs et al., 1998) at cGMP concentrations in excess of 3 mM.

The interpretation of the above experiments is complicated, however, by the possibility of ligand binding to the mutant subunits, especially at higher concentrations of cGMP. Evidence for such an effect is suggested by the fact that dose response plots of P_O as a function of ligand concentration for some heteromultimers do not reach a saturating value, even at 30 mM cGMP. Indeed, when we estimate the effect of binding to mutant subunits using the MWC model (see Experimental Procedures), we predict that there would be significant effects of binding to subunits that contain the R559E mutation at concentrations of cGMP above 1 mM (especially for channels containing three functional binding sites), despite the greater than 2000-fold decrease in apparent affinity. Hence, we proceeded to make a second mutation in the binding domain.

Use of Double Point Mutations to Abolish Ligand Binding to Mutant Subunits

To decrease further the agonist affinity of mutant subunits, we created the double mutant RET/EA, in which we mutated threonine 560 to alanine, in conjunction with the R559E mutation. In RET, the T560A mutation increases the $K_{1/2}$ with cGMP by 28-fold and produces a small (≤5-fold) decrease in P_{max} (Altenhofen et al., 1991; Varnum et al., 1995). If the effects of the R559E and T560A mutations on cGMP binding energy are additive, then the $K_{1/2}$ for activation of homotetrameric channels should be increased at least 30,000-fold, to >1.5 M. Thus, binding of cyclic nucleotide to RET/EA subunits should be insignificant within the range of concentrations that we tested (30 μM–30 mM). The effectiveness

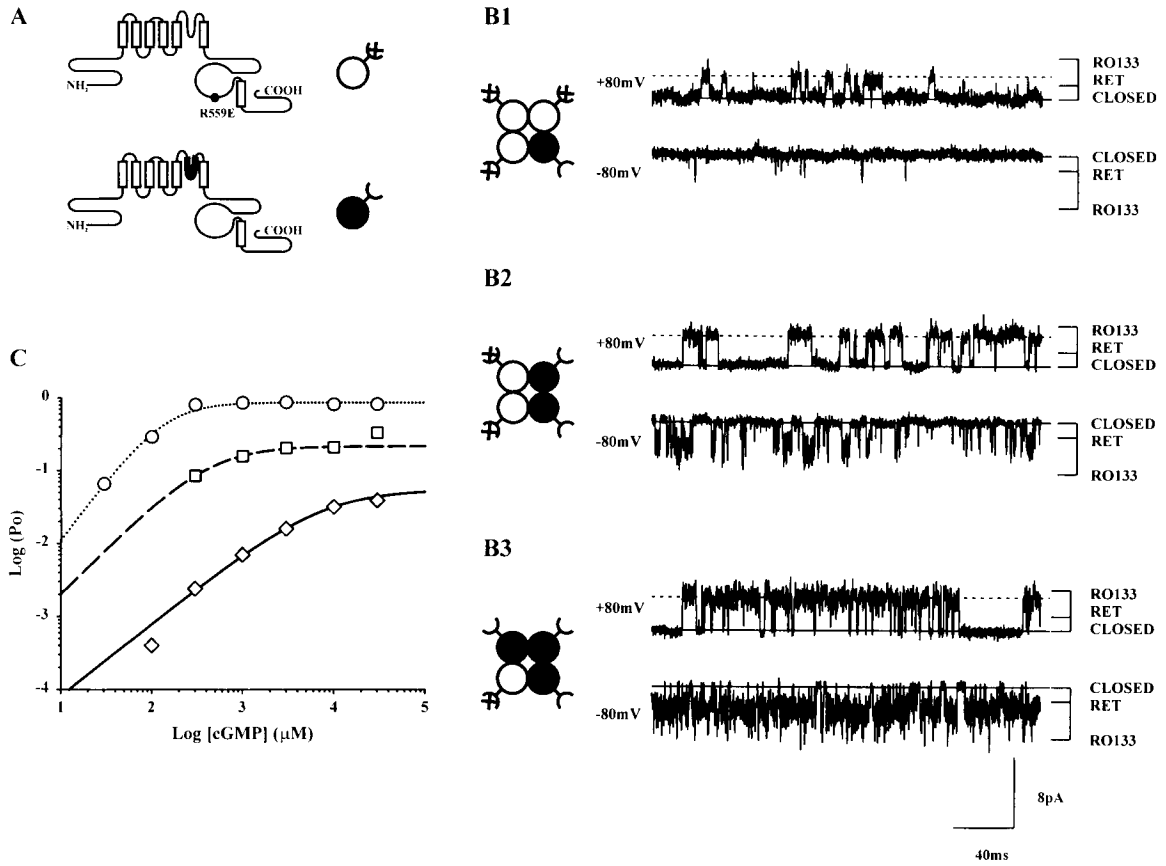

Figure 3. Coexpression of RET/E with RO133 Subunits Yields Channels with Intermediate Conductance and Reduced Maximal Open Probability

(A) Schematic representation of the RET/E and RO133 subunits.

(B1–B3) Recordings from separate single-channel patches following coexpression of RET/E and RO133 monomeric subunits. Data were obtained at +80 mV in the presence of 30 mM cGMP (top traces) and −80 mV and 3 mM cGMP (bottom traces). The graphic to the left of each pair of traces gives the subunit stoichiometry assigned to each channel on the basis of its conductance (26, 42, and 47 pS in B1, B2, and B3, respectively).

(C) Dose response curves for the channels shown in B1 (diamonds), B2 (squares), and B3 (circles). The lines are fits of the Hill equation to the probabilities determined at concentrations of cGMP between 0.03 mM and 10 mM.

of the double mutation in preventing channel activation is supported by the finding that neither the ROON-S2/EA nor the RET/EA subunits form channels that can be activated by cyclic nucleotides. However, when RET/EA subunits are coexpressed with RO133 subunits, channels of all expected intermediate conductance classes with reduced P_O values are observed (Figure 4).

The very low P_{max} values of some of the heteromultimeric channels make it difficult to measure reliably either their single-channel conductance or the number of channels in the patch. Therefore, we routinely measure these parameters under conditions where open probability is enhanced by applying cGMP in the presence of 10 μM Ni^{2+}, which selectively stabilizes the open state of the channel (Gordon and Zagotta, 1995a). For each channel, we first determined its dose response curve for activation by cGMP in the absence of Ni^{2+} and then determined single-channel conductance in the presence of 30 mM cGMP plus Ni^{2+}. As shown by the individual dose response curves of Figure 4C, P_O clearly saturates at relatively low concentrations of cGMP, allowing us to determine P_{max}. The continuous increase in P_O at high cyclic nucleotide concentrations seen in some of the RET/E:RO133 coexpression experiments is no longer evident. This suggests that the functional binding domain is saturated with ligand and that even at 30 mM cGMP, the mutant subunits do not bind cGMP and do not contribute to ligand-dependent gating.

The relation between P_{max} (as estimated from P_O at 10 mM cGMP) and single-channel conductance from all the individual RET/EA:RO133 coexpression experiments is plotted in Figure 5B. There is a clear trend for channels with larger conductances, and hence greater numbers of RO133 subunits bearing functional binding sites, to exhibit higher P_{max} values. The channels fall into three distinct conductance classes, each with distinct P_{max} values. Because these conductance clusters are similar to those observed upon coexpression of RET and RO133 subunits with wild-type binding sites (Figure 5A), we have assigned each class to a distinct subunit stoichiometry. Thus, we conclude that the class of channels with conductances of 25–32 pS and P_{max} values of

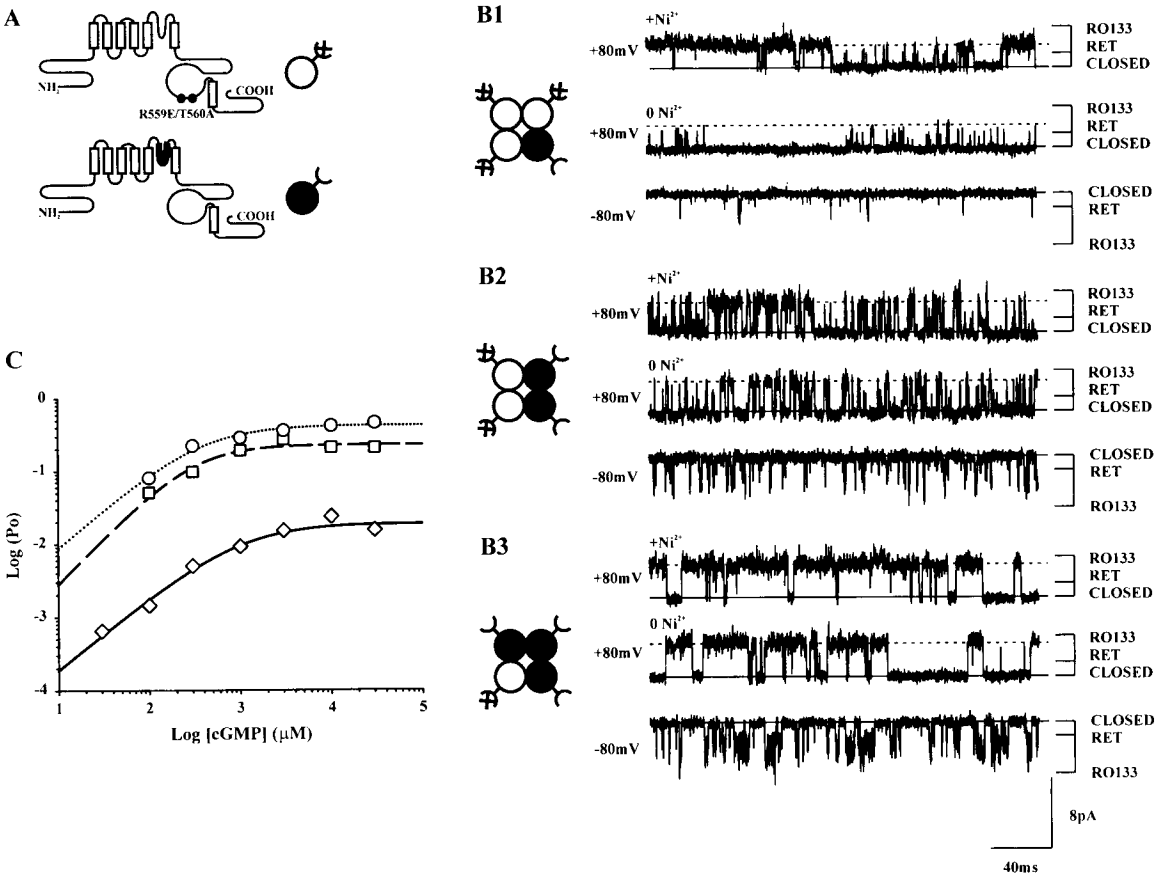

Figure 4. Coexpression of RET/EA with RO133 Subunits Yields Channels with Intermediate Conductances and Reduced Maximal Open Probabilities

(A) Schematic representation of the RET/EA and RO133 subunits.

(B1–B3) Recordings from separate single-channel patches following coexpression of RET/EA and RO133 monomeric subunits. The top traces are from recordings at +80 mV in the presence of 30 mM cGMP and 10 μM Ni^{2+}, while the bottom pair of traces were obtained in the presence of 30 mM cGMP in the absence of Ni^{2+} at ±80 mV, as indicated. The graphic to the left of the traces gives the subunit stoichiometry assigned to each channel on the basis of its conductance (32, 40, and 47 pS in B1, B2, and B3, respectively).

(C) Dose response curves for the channels shown, B1 (diamonds), B2 (squares), and B3 (circles). The lines are fits of the Hill equation to the probabilities determined at concentrations of cGMP between 0.03 and 30 mM (−80 mV, absence of Ni^{2+}).

around 0.017 are composed of 1 RO133 and 3 RET/EA subunits (Figure 5B, diamonds, n = 7), channels with conductances of around 36–43 pS and P_{max} values of around 0.16 are composed of 2 RET/EA and 2 RO133 subunits (Figure 5B, squares, n = 8), and channels with conductances of 47–49 pS and P_{max} values of around 0.32 are composed of 1 RET/EA and 3 RO133 subunits (Figure 5B, circles, n = 7).

Mean dose response curves (P_O versus cGMP concentration) for channels with the same subunit composition were obtained by averaging P_O values at each cGMP concentration. These data are plotted in Figure 5C for each of the three subunit stoichiometries. In all cases, the dose response relations saturate at millimolar concentrations of cGMP. A fit of the Hill equation indicates that channels from the lowest intermediate conductance class show a Hill coefficient near 1, consistent with the view that these channels contain only a single binding site. Channels from the two larger intermediate conductance classes, which should contain more than one functional binding site, show steeper dose response relations, as expected.

Conductance Levels Accurately Report Stoichiometry of Channels with Mutant Subunits

The above approach assumes that single-channel conductance provides a reliable fingerprint of subunit stoichiometry that is solely a function of P region composition and is independent of the gating state of the channel. Thus, channels with three RET and one RO133 P regions are assumed to have a conductance of ~27 pS, regardless of whether the channels have one or four functional binding sites. However, Ildefonse and Bennett (1991) and Taylor and Baylor (1995) reported that native CNG channels tend to open to a subconductance state at low cyclic GMP concentrations where P_O is low. More recently, Ruiz and Karpen (1997) reported similar behavior for channels expressed from RET subunits in *Xenopus* oocytes. While other studies have concluded that the subconductance states of CNG channels are largely

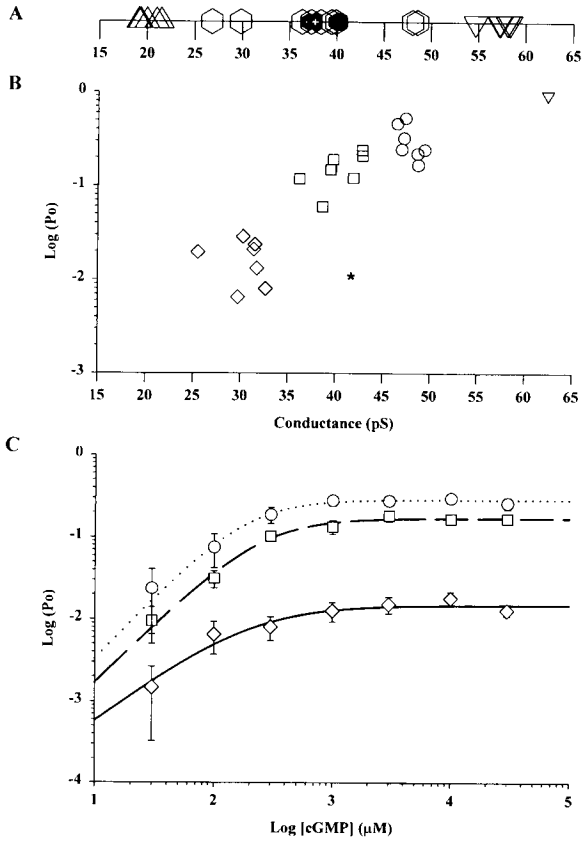

Figure 5. Relationship of Maximal Open Probability and Single-Channel Conductance Reveals Three Classes of Intermediate Gating Properties, Corresponding to Channels with One, Two, or Three Functional Binding Sites

(A) One-dimensional scatter plot of conductances for homotetrameric RET, homotetrameric RO133, and heteromultimeric channels with intermediate conductances (replotted from Figure 2D).

(B) Scatter plot of open probability at 10 mM cGMP as a function of conductance when RET/EA (small conductance subunit with mutant binding site) is coexpressed with RO133 (large conductance subunit with wild-type binding site). Three classes of intermediate conductance channels, which cluster around distinct P_{max} values, are observed. Class 1 (open diamonds), subunit stoichiometry of 3RET/EA:1RO133. Class 2 (open squares), subunit stoichiometry of 2RET/EA:2RO133 in both *cis* and *trans* arrangements. Class 3 (open circles), subunit stoichiometry of 1RET/EA:3RO133. One channel has the conductance and open probability of homomeric RO133 (open inverted triangle). Channel indicated by asterisk is not included in mean dose response analysis (see text).

(C) Mean dose response curves for each of the above three classes of heteromultimeric channels. Symbols as in (B). (n = 7 patches for each class; not all points determined in each patch.) Bars show standard errors. The lines are Hill fits to the data points at each concentration. The P_{max}, $K_{1/2}$, and Hill coefficient values are as follows: class 1, 0.015, 190 μM, 1.1; class 2, 0.170, 250 μM, 1.43; and class 3, 0.285, 190 μM, 1.52.

due to proton block of the pore and are unrelated to gating of the channel (Goulding et al., 1992; Root and MacKinnon, 1994; Bucossi et al., 1997), we were concerned that the presence of subconductance states might have caused us to misidentify the subunit composition of the channels. Such a possibility is suggested by the conclusion of Ruiz and Karpen (1997) that channels with two ligands bound exhibit a low P_{max} (0.01) and open primarily to a subconductance state. Thus, our 27 pS channels (P_{max} = 0.015), which we interpret as being composed of one RO133 and three RET/EA subunits, might actually represent the opening of channels composed of two RO133 and two RET/EA subunits to a subconductance state.

Although complications introduced by gating-dependent subconductance states should be minimized by our use of Ni^{2+} to enhance channel open probability, we took two additional approaches to address this issue more directly. First, we mutated the binding site in the RO133 subunits and coexpressed them with wild-type RET subunits, the reverse arrangement of the previous experiments. If channel conductance accurately reflects P region stoichiometry independent of channel gating, we would expect that channels with three mutant RO133 subunits and one wild-type RET subunit would exhibit a large conductance (48 pS) and low P_{max}. Conversely, if our conductance measurements were distorted by gating-dependent subconductance states, we would expect that channels with the lowest P_{max} values should enter primarily a subconductance state that is significantly less than 48 pS. Because RO133/EA double mutant subunits did not express, we coexpressed RO133/E and RET subunits.

Although the RO133/E subunits do not yield channels that can be activated by cyclic nucleotide when expressed on their own, channels of intermediate conductances are observed when RO133/E subunits are coexpressed with RET subunits (Figure 6B, closed symbols). Moreover, these channels are clustered in three classes whose intermediate conductances are similar to those seen when RO133 subunits with a wild-type binding site are coexpressed with either wild-type RET subunits (Figures 2 and 6A) or RET/EA subunits (Figures 5B and 6B, open symbols). However, in contrast to channels formed from RET/EA and RO133 subunits, here the channels with the largest intermediate conductances (48 pS) now display the lowest P_{max} values. Conversely, channels with the smallest intermediate conductance (26 ± 1 pS) exhibit the greatest P_O. Channels in the middle conductance class (35–40 pS) display intermediate P_{max} values. Importantly, we do not observe 27 pS channels with a low P_{max}, as would be expected if channels containing two RET and two RO133 P regions and only two functional binding sites do indeed open with a low P_{max} to a subconductance state (e.g., Ruiz and Karpen, 1997).

Our second approach uses tandem dimers to constrain subunit stoichiometry and order around the central pore. Thus, we expect that channels formed from RO133-RET/EA heterodimers should contain two RO133 and two RET/EA subunits in the *trans* arrangement and thus display a conductance of around 37 pS and a P_{max} of around 0.17. As shown in Figure 6C, this was indeed observed for the majority of such channels (8 out of 11; mean conductance 35 ± 1 pS, P_{max} = 0.15 ± 0.02). A minority of channels (3 of 11) exhibited a bursting behavior with high P_{max} and lower than expected conductance. Although the nature of this behavior is unclear, the heterodimer data confirm that channels with only two functional binding sites activate with a relatively high P_{max} (>0.15) and support the assignment in the monomer

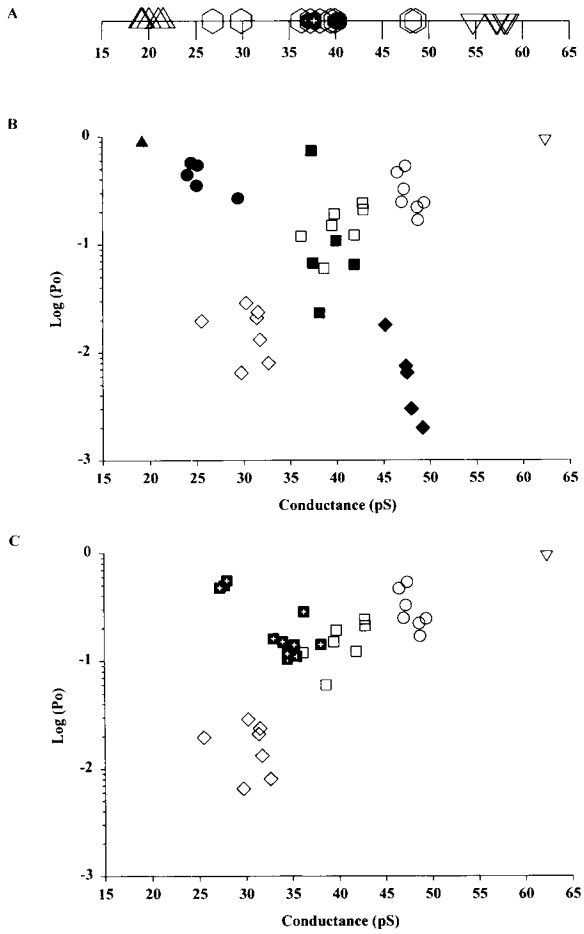

Figure 6. Channel Conductance Accurately Reflects Subunit Stoichiometry Independent of Channel Gating Properties

(A) One-dimensional scatter plot of conductances for homotetrameric RET, homotetrameric RO133, and heteromultimeric channels with intermediate conductances (replotted from Figure 2D).

(B) Scatter plot of P_{max} values determined at 10 mM cGMP as a function of channel conductance when RO133/E (large conductance subunit with a mutated binding site) is coexpressed with RET (small conductance subunit with a wild-type binding site). For comparison, the data from Figure 5B obtained upon coexpression of RET/EA (small conductance subunit with mutated binding site) and RO133 (large conductance wild-type binding site) are replotted (open symbols). Three classes of channels with intermediate conductances are observed: Class 1 (closed circles), 3 RET : 1 RO133/E subunits. Class 2 (closed squares), 2 RET : 2 RO133/E subunits in both *cis* and *trans* arrangements. Class 3 (closed diamonds), 1 RET : 3 RO133/E subunits. One channel has the conductance and open probability of homomeric RET (closed triangle).

(C) Scatter plot of open probability at 10 mM cGMP as a function of conductance for channels observed upon expression of RO133-RET/EA tandem heterodimers (closed squares with open plus symbols). Data from Figure 5B are again replotted for comparison.

mixing experiments that the 37 pS channels are composed of two RO133 and two RET/EA subunits.

Dependence of Opening Equilibrium on the Number of Functional Binding Sites

Since channel conductance appears to report subunit stoichiometry reliably, we averaged the P_{max} values for all channels within a given conductance class and plotted these mean values as a function of the number of wild-type binding sites per channel (Figures 7A1, 7B1, and 7C1). The P_{max} values have also been converted to effective equilibrium constants, L_{eff}, for the open to closed reactions: $1/L_{eff} = \Sigma[\text{open states}]/\Sigma[\text{closed states}] = P_{max}/(1 - P_{max})$ (Figures 7A2, 7B2, and 7C2). Included in these figures are values for P_{max} and $1/L_{eff}$ for a channel with four wild-type binding sites (based on measurements of RO133 homotetramers) and the values expected for a channel with no functional binding sites (based on our experimental measurements of the spontaneous, ligand-independent open probability of RO133 channels; $P_O = 1.25 \times 10^{-4}$; Tibbs et al., 1997).

These data show that the binding of even a single ligand is sufficient to produce significant activation of the channel, increasing channel open probability and $1/L_{eff}$ ~120-fold above the spontaneous open probability. There is then a progressive increase in maximum open probability as the number of wild-type binding sites per channel increases, although the effectiveness of successive ligand binding events in increasing open probability varies as a function of the number of ligands bound. Thus, the second binding event causes only a 12-fold increase in $1/L_{eff}$ whereas the third binding event has an even smaller effect, increasing $1/L_{eff}$ by an additional factor of only 2. The fourth binding event, in contrast, produces a large increase of 40-fold in this opening equilibrium. As we will discuss below, these data are inconsistent with either the concerted MWC model or models in which each subunit activates independently, which predict much more uniform increases in channel opening upon successive ligand bindings. The very small increment in channel opening upon going from two to three ligands bound is particularly striking and forms the basis for a model for channel gating, which we propose below.

MWC and Independent Models Are Not Consistent with Heteromultimer Gating Properties

Two extreme schemes, the independent subunit model and the MWC model (Figures 8A and 8B; see Theory section of Experimental Procedures), have been used to explain how the various subunits of the multimeric CNG channels contribute to activation gating (Stryer, 1987; Goulding et al., 1994; Varnum and Zagotta, 1996; Li et al., 1997; Tibbs et al., 1997). In both the independent subunit and MWC models, channel subunits undergo an allosteric gating reaction between a resting (or closed) and active (or open) state. In accord with the original nomenclature of the MWC model, we designate the resting state of a subunit T (for tense) and the active state of the subunit R (for relaxed). Furthermore, in accord with experimental results, this allosteric gating reaction can occur even in the absence of agonist (Picones and Korenbrot, 1995; Tibbs et al., 1997). Both models also assume that when a subunit is in the active state, it binds ligand with a higher affinity (dissociation constant = K_R) compared to the affinity of the resting or tense state (K_T). As a result of the increased affinity for ligand of the active state, ligand binding increases the equilibrium between resting (T) and active (R) states by a factor

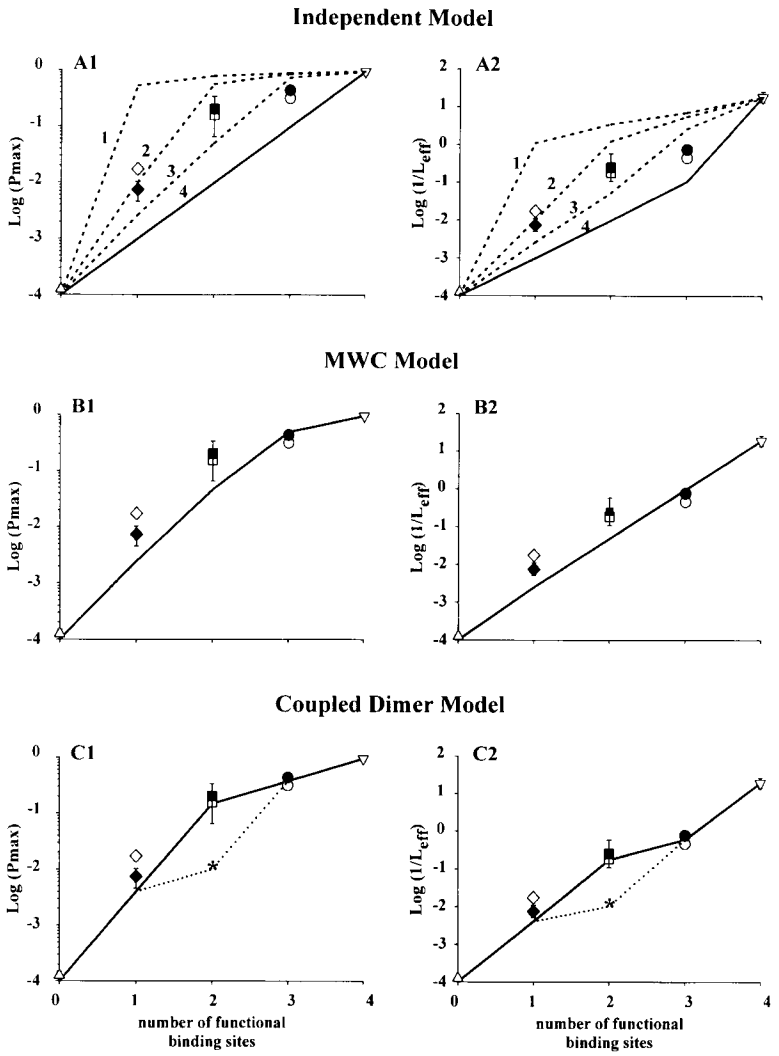

Figure 7. Dependence of Channel Gating Properties on the Number of Functional Binding Sites Is Inconsistent with Simple MWC or Independent Gating Models but Suggests that Channels Gate as Two Independent Dimers

Each of the three pairs of panels compares the predictions of the indicated channel gating model ([A], independent; [B], MWC; [C], coupled dimer) to the measured ability of the channel to gate with 0–4 functional ligand-binding sites. In each case, the left panel (A1, B1, and C1) plots Log(P_{max}) as a function of the number of wild-type binding sites per channel. Mean P_{max} values for each channel class observed upon coexpression of either RET/EA and RO133 subunits (open symbols) or RET and RO133/E subunits (closed symbols) are shown. Bars show standard errors of measurements. The right panel (A2, B2, and C2) plots Log($1/L_{eff}$) as a function of the number of wild-type binding sites per channel. Symbols are as described above.

(A1 and A2) The solid line shows the predictions of the independent model in which the channel opens when all four subunits have activated. The dotted lines show the predictions of the independent models that allow for a channel to open when one, two, or three subunits have activated (as labeled).

(B1 and B2) The line represents the predicted values from MWC concerted allosteric model.

(C1 and C2) The lines represent the predicted values of the coupled dimer model. The model predicts two distinct P_{max} values for channels containing two wild-type and two mutant CNB sites depending on whether both functional binding sites lie in the same functional dimer (dashed line) or different functional dimers (solid line). The asterisk shows the P_{max} value for the channel in Figure 5B similarly marked.

equal to K_R/K_T, thus stabilizing the channel in the active, open conformation, causing an increase in channel open probability. The two models differ, however, in terms of how the activation reactions of each individual subunit are coupled.

According to the independent subunit model (Figure 8A; see Experimental Procedures), each subunit undergoes a separate allosteric gating transition between the resting (T) and active (R) state that is independent of the activation state of the other subunits in a channel. In the simplest version of this model, a channel is only open when all four of its subunits are in the active (R) state, similar to the Hodgkin-Huxley gating scheme. For simplicity, we assume that each ligand binding event is identical and independent, reflecting the fact that the channels we study are homotetramers with four identical ligand-binding sites. In contrast to the independent subunit model, the MWC model postulates that the four subunits of the channel undergo a concerted allosteric transition between a single closed (T) and a single open (R) state (Figure 8B). Although the four subunits activate in concert, each subunit binds ligand independently and equivalently.

The predictions of both the MWC model and the independent subunit model as to how P_{max} varies as a function of the number of subunits with wild-type binding sites are compared with our experimental results in Figure 7. The predictions of both models are completely constrained by measurements for wild-type homomeric channels of spontaneous open probability in the absence of agonist (Tibbs et al., 1997) and maximum open probability in the presence of a saturating agonist concentration (Tibbs et al., 1998). No free parameters are required in either model.

The experimental data deviate significantly from both the independent model (Figures 7A1 and 7A2) and the MWC model (Figures 7B1 and 7B2). One modification of the independent model, previously proposed by Varnum and Zagotta (1996), is that channels can open when fewer than four subunits have activated. However, the data are also inconsistent with the three possible modifications of the independent model, in which channel

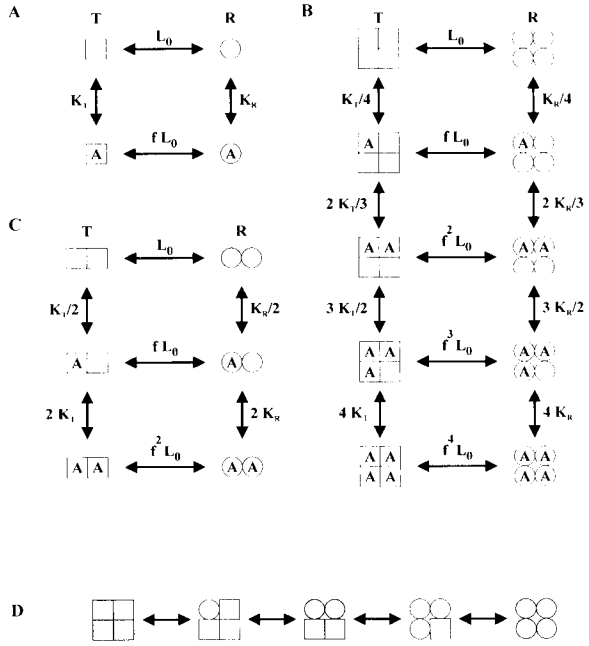

Figure 8. Schemes for Activation Gating of Tetrameric CNG Channels

(A) The independent model. Each subunit of the tetramer can undergo, independently, a conformational change between a resting T state (square) and an active R state (circle) and bind one agonist molecule (A), with dissociation constants K_T and K_R, respectively. A single subunit is shown. In the four separate versions of this model we consider, channel opening requires that four, three, two, or one subunits activate. In (A), (B), and (C), f equals K_R/K_T.

(B) The MWC model. All four subunits undergo a single, concerted allosteric change between the resting T state and active R state (which correspond to the closed and open states of the channel, respectively). Channels can undergo transitions between these states with 0–4 ligands bound, represented by the five rows.

(C) The coupled dimer model. Both subunits within a dimer undergo a concerted transition between a resting T and active R state. Each subunit within a dimer binds ligand independently of the other subunit. A single dimer is shown, and the channel is composed of two such functional dimers operating independently. A channel is only open when both dimers are in the R state.

(D) Activation states for the four subunits of a channel during the unliganded opening reaction. In the independent model, all five states are permitted. In the MWC model, only the extreme left and right states are allowed. In the coupled dimer model, the three shaded states are permitted.

opening requires that only one, two, or three subunits enter the active state (Figures 7A1 and 7A2).

Coupled Dimer Model Provides a Good Description of Gating Properties

In contrast to the poor fits to the experimental data provided by the independent and MWC models, a hybrid of these two schemes, which treats the tetrameric channel as a dimer of dimers, shows excellent correspondence with the gating properties observed. In this model (Figure 8C), the two subunits that comprise a dimer undergo a concerted (MWC-like) allosteric transition between a resting and active state, which is coupled to an increase in affinity of each subunit for agonist. As in the MWC model, each ligand binding event is independent and identical. However, unlike the MWC model but similar to the independent model, the two dimers that comprise a channel activate independently, and the channel is only open when both dimers enter the active state.

Because the two dimers that make up the channel activate independently, there is no longer necessarily a linear relation between number of ligands bound and opening equilibrium. In particular, the dimer model accounts for the relatively small increase in open probability between channels with two ligands or three ligands bound (because the opening of the dimer with only one functional binding site is the limiting factor).

An interesting consequence of this model is that there are two distinct functional configurations of the binding sites in a channel that contains two RET/EA and two RO133 subunits in the *cis* arrangement. Thus, a subunit containing a wild-type binding site could form a functional dimer with either its neighboring subunit, which contains a wild-type binding site, or with its other neighboring subunit, which contains a mutant binding site. In the former case, the channel would contain one dimer that possesses two functional binding sites and one dimer that possesses no functional binding sites. In this case, channel opening is limited by the low activation probability of the dimer with two mutant subunits, and the channel is predicted to exhibit a very low P_{max} value (Figure 7C, dashed lines), only slightly greater than that expected for a channel with only one functional binding site. If, on the other hand, a wild-type subunit pairs with a mutant subunit, then each dimer will contain one functional binding site. In this case, ligand binding will enhance the probability of opening of each dimer, and the channel is predicted to display a relatively high P_{max} of around 0.2 (Figure 7C, solid lines).

To explore the gating properties of channels with two RET/EA subunits and two RO133 subunits in the *cis* arrangement, we coexpressed RET/EA-RET/EA tandem homodimers with RO133-RO133 tandem homodimers, which constrains the two mutant subunits to lie next to each other. Of the 13 intermediate conductance channels we observed, 9 exhibited low P_{max} values (mean = 0.034 ± 0.010, n = 9; Figure 9A) that were considerably less than the P_{max} values observed above with tandem heterodimers (Figure 6C). Surprisingly, the low P_{max} channels were not potentiated by Ni^{2+}. As a result, the P_{max} values provide an upper limit for the true values since we could not reliably determine the number of channels in these patches. The other four channels had higher P_{max} values (Figure 9B), similar to those observed in the RET/EA-RO133 heterodimer expression experiments (Figure 6C), consistent with the formation of channels with one functional binding site per dimer. The fact that the majority of channels expressed from tandem homodimers had low P_{max} values suggests that the subunits in a tandem dimer tend to associate together to form a stable, functional dimer.

In the monomer coexpression studies shown in Figure 5B, all the channels with conductances consistent with the 2 RO133: 2 RET/EA subunit stoichiometry (35–42 pS) showed relatively high P_{max} values, suggesting that

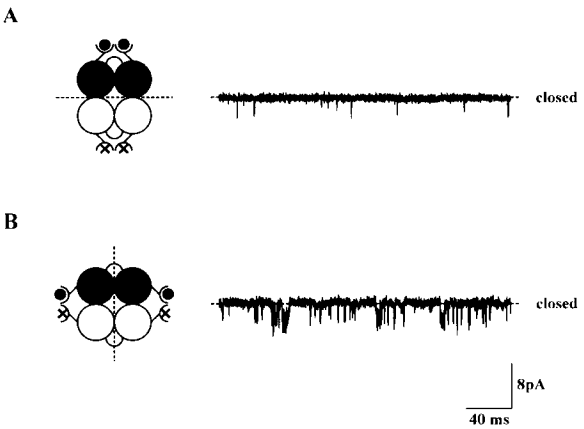

Figure 9. Coexpression of RET/EA-RET/EA Tandem Homodimers with RO133-RO133 Tandem Homodimers Yields Two Populations of Channels with Either High or Low P_{max} Values

(A) Recording from a patch containing cyclic nucleotide–activated channel(s) with a stable, low P_{max}. This channel was not potentiated by Ni^{2+}, and hence, the number of channels in this patch is not known; the upper limit estimate for P_{max} is 0.01. The cartoon illustrates a proposed subunit arrangement in which one functional dimer contains two wild-type binding sites (contributed by the RO133-RO133 tandem homodimer, closed circles), and the other functional dimer contains two mutant binding sites (contributed by the RET/EA-RET/EA tandem homodimer, open circles). The dashed line indicates the axis of symmetry, showing that the channel assembles with each functional dimer corresponding to one of the tandem homodimers.
(B) Recording from a patch containing a single channel with a stable P_{max} of 0.34. Here we propose that the channel assembles so that each functional dimer contains one mutant subunit (contributed by the RET/EA-RET/EA tandem homodimer) and one wild-type subunit (contributed by the RO133-RO133 tandem homodimer).
Both recordings were performed at −80 mV in the presence of 30 mM cGMP.

the two functional dimers that comprise these channels each contained one wild-type binding site. However, we did observe a class of channels whose properties resembled those of the majority of channels seen in the homodimer coexpression studies (i.e, low P_{max} values and resistance to potentiation with Ni^{2+}). Most of these channels could not be included in the data shown in Figure 5B because we could not accurately determine their conductance, and hence subunit stoichiometry, due to their resistance to potentiation with Ni^{2+}. However, one of these channels did eventually potentiate upon prolonged exposure to Ni^{2+} (channel marked by asterisk in Figure 5B), revealing single-channel conductance of 41 pS, consistent with a stoichiometry of two RET/EA and two RO133 subunits in the *cis* configuration. Moreover, the low P_{max} value of this channel (~0.01) is similar to the low P_{max} values seen with the majority of the channels upon coexpression of the tandem homodimers. Taken together, the above observations, showing a mix of high and low P_{max} values for channels with two functional and two nonfunctional binding sites, are consistent with the predictions of the coupled dimer model.

Discussion

By coexpressing channel subunits with functional and nonfunctional cyclic nucleotide–binding sites and using single-channel conductance as an independent tag to determine subunit stoichiometry, we have measured the contribution of each of four ligand binding events to the activation of CNG channels. Our results indicate that the binding of a single ligand is sufficient to produce a significant increment in channel open probability. Each additional ligand binding step causes an incremental increase in channel open probability, although with varying efficacy.

An underlying assumption in our studies is that the mutations in the cyclic nucleotide–binding site of one subunit affect only the ability of that subunit to bind ligand and do not alter the agonist-independent allosteric gating reaction of the channel (i.e., L_0). This is important because our quantitative analysis assumes that channels with different numbers of wild-type and mutant subunits differ only in the maximal number of ligands bound and not in the efficacy with which any given bound agonist activates the channel.

For the R559E mutation, there is strong evidence that the above assumption is valid. Thus, we find that a wide range of amino acid substitutions at this position (including R559E) has little effect on gating, (i.e., P_{max}), despite their ability to decrease sensitivity to ligand (Tibbs et al., 1998). Moreover, mutation of this arginine to a glutamine decreases ligand sensitivity >28-fold with no change in L_0 as determined from spontaneous open probability (Tibbs et al., 1997). In the case of T560A, the situation is less clear as this mutation does cause a small decrease in P_{max} (≤5-fold) in addition to decreasing ligand sensitivity (Varnum et al., 1995). This effect could arise from a change in either the allosteric gating equilibrium of the channel (L_0) or in the ratio of the agonist affinity of the open versus closed state of the channel (i.e., K_R/K_T). The insensitivity of L_0 to mutation of the neighboring R559 residue suggests that the T560A mutation may act to alter the K_R/K_T ratio. This conclusion is also supported by our finding that the P_{max} values for channels containing two wild-type and two mutant subunits were similar irrespective of whether the mutant binding pocket had the R559E mutation alone or in combination with T560A.

Our results are in qualitative agreement with those of Ruiz and Karpen (1997) in showing a progressive increase in channel activation with increasing numbers of bound ligands. However, there are also certain differences. Ruiz and Karpen (1997) used an elegant approach in which light activation of a cGMP analog covalently tethered variable numbers of agonists to homomeric RET channels expressed in oocytes. The authors noted four types of changes in channel activation properties following UV illumination, which they interpret as representing channels with 1–4 ligands attached. They concluded that tethering the first agonist causes no measurable increase in channel opening by itself but shifts the dose response curve for channel activation in response to subsequent cGMP applications to lower concentrations. Tethering the second ligand causes the channel to open to a small extent, with a P_O of 0.01. Attachment of the third ligand produces a larger increase in P_O to 0.3, whereas tethering the fourth ligand fully opens the channel. This differs from our data, which show clear activation by a single ligand (P_{max} = 0.017) and even

more significant activation by two (P_{max} = 0.16) or three (P_{max} = 0.32) bound ligands.

The discrepancy between our results and those of Ruiz and Karpen, especially in terms of the efficacy of a single agonist, could reflect some unforeseen allosteric effect of our binding site point mutations on channel gating, although this seems unlikely as discussed above. Alternatively, our results can be reconciled with those of Ruiz and Karpen if we shift their assignments of the number of attached ligands downward by 1. The tethered agonist approach relies on differences in the functional properties of channels following illumination to count the number of tethered agonists. However, our finding that channels with two or three ligands bound exhibit very similar P_{max} values, around 0.2–0.4, might cause channels with two or three tethered agonists to be grouped into a single functional class, which would correspond to the class that the authors associate with three agonists bound. The next functional class of channels they observe, with a P_O of 0.01, which they associate with channels having two ligands bound, would then correspond to channels with only one tethered agonist, in good agreement with our data on channels with only one functional binding site (P_{max} = 0.017). This scenario does not explain the class of channels they report, which shows an enhanced ligand sensitivity but no increase in basal P_O and which the authors ascribe to channels with only one tethered agonist. However, both native CNG channels (Gordon et al., 1992) as well as RET channels expressed in oocytes (Molokanova et al., 1997; our own unpublished data) often show spontaneous increases in cGMP sensitivity due to channel dephosphorylation upon patch excision, complicating the interpretation of the number of ligands tethered based on changes in apparent affinity.

We compared our data with the predictions of two extreme models for how the individual subunits of a CNG channel contribute to activation gating. Our data were inconsistent with either the MWC model, in which the four subunits undergo a single, concerted allosteric conformational change, or models similar to the Hodgkin-Huxley scheme in which each subunit gates independently. We could, in principle, improve the fits with these models by relaxing the requirement that each subunit behave identically and adjust the equilibrium constants for each subunit arbitrarily to fit the data. However, such an approach seems unattractive given that the channels function as homotetramers. Moreover, such fits to the data would require that successive ligand binding events contribute highly nonmonotonic free energy changes toward activation gating.

The data are, however, consistent with a hybrid version of the MWC and independent subunit schemes in which the four subunits of the channel gate as two coupled dimers. The two subunits within a dimer undergo a concerted transition between the resting and active conformation, as in the MWC model. Each dimer, however, activates independently, and a channel is only open when both dimers enter the active state, similar to the independent scheme. The coupled dimer model provides a good fit to the observed P_{max} values and each of the opening equilibria ($P_{max}/(1 - P_{max})$) upon coexpression of wild-type subunits and subunits with mutated binding domains. Moreover, the model is also consistent with the observation of two distinct classes of gating properties for channels containing two wild-type and two mutant subunits in the *cis* arrangement.

The coupled dimer model is also consistent with a physical model for ligand gating that we previously proposed (Goulding et al., 1994), based on the X-ray crystal structure of the homologous cAMP-binding sites of the bacterial catabolite activating protein, CAP (Weber and Steitz, 1987). According to this model, channel opening is due to a quaternary change in subunit–subunit orientation, which is allosterically coupled to a change in orientation between two cyclic nucleotide–binding sites on neighboring subunits. This change in binding site orientation is proposed to permit the formation of intersubunit bonds between the ligand bound to one subunit and the C helix region of the binding site of the neighboring subunit. This view is consistent with the role of the C helix in forming intersubunit ligand contacts in CAP homodimers and with the finding that the C helix of CNG channels makes important contacts with agonist that are crucial for ligand-gating (Goulding et al., 1994; Varnum et al., 1995). In the coupled dimer model, activation of a dimer would permit each subunit to form intersubunit bonds with ligand bound to its neighboring subunit, thus preferentially stabilizing the ligand bound to the active state of the dimer. The view that channel gating involves the formation of intersubunit ligand bonds is consistent with data on the nicotinic acetylcholine receptor, where a single ACh molecule interacts with distinct sites on neighboring subunits (Czajkowski and Karlin, 1991).

The view that the tetrameric CNG channels may exist as two dimers, and thus exhibit 2-fold rather than 4-fold symmetry, is also consistent with the structure of other tetrameric proteins such as hemoglobin (Perutz et al., 1987; Royer et al., 1995). Dimeric assembly is also likely to occur for the ClC family of chloride channels (Ludewig et al., 1996; Middleton et al., 1996) and the two-pore family of potassium channels (Ketchum et al., 1995). Two previous studies on CNG channels also suggest a 2-fold symmetry. First, Root and MacKinnon (1994) demonstrated that the four pore-forming P regions of the catfish olfactory channel interact to form two identical proton binding sites, with each site being formed by two identical glutamate residues (E333 in catfish olfactory channel) contributed by two subunits. Second, Gordon and Zagotta (1995b) showed that the Ni^{2+} binding site involved in channel potentiation is formed by two identical histidine residues (H420 located after S6) on neighboring subunits. This latter finding is also consistent with the idea that the carboxyl termini of two neighboring subunits within the channel are in close proximity to each other. Furthermore, the notion that the tetrameric CNG channels may activate as functional dimers is consistent with data on subunit assembly of the homologous voltage-gated K channels (Tu and Deutsch, 1998, Biophys. J., abstract). There it has been proposed that the tetrameric K channels are first assembled as dimers and then the dimers associate to form tetramers. Given the similarity in structure between the K channels and CNG channels, it is possible that a coupled-dimer model of channel activation may also apply to other members of the voltage-gated channel superfamily.

Experimental Procedures

Molecular Biology

The bovine rod photoreceptor cyclic nucleotide–gated channel subunit 1 cDNA (RET) was subcloned in a modified vector pGEM-3Z (Promega) containing the 5′ and 3′ *Xenopus* β-globin untranslated sequences flanking the polylinker region (Liman et al., 1992; Goulding et al., 1993). The P region chimera (RO133) and point mutants were made using polymerase chain reaction and subcloning strategy (PCR, Goulding et al., 1993; Tibbs et al., 1998). The resulting cDNA clones were verified by dideoxy chain termination sequencing of the PCR fragment. Arg-559 of RET was mutated to a glutamate to make the clone, RET/E. A fragment containing the mutation from RET/E cDNA was obtained by digestion with NsiI and HindIII and subcloned into the RO133 vector, making the cDNA clone, RO133/E. PCR and subcloning were then performed with RET/E as the template for making the double mutant, RET/EA, where Thr-560 was mutated to an alanine. RNA was transcribed from either NheI-linearized or HindIII-linearized DNA using T7 RNA polymerase (Message Machine, Ambion) and injected into *Xenopus* oocytes prepared as previously described (Goulding et al., 1992).

The dimer constructs were made using PCR and subcloning (Liu et al., 1996). RO133-RET/EA heterodimer was made by digesting RET/EA with SalI and HindIII, gel isolating the 1.6 kb fragment, and subcloning the fragment into RO133DV (Liu et al., 1996). RO133-RET/EA was verified by size of linearized plasmid and restriction digestion with SalI and HindIII. RET/EADV was made by digestion of RET/EA with NsiI and ApaI and subcloning the fragment into RETDV. RET/EA-RET/EA homodimer was made by subcloning the SalI/HindIII fragment of RET/EA into the RET/EADV. The constructs were amplified in the SURE2 bacteria cell line (Stratagene). Due to possible recombination events in the bacteria and monomer contamination, DNA was gel-purified twice post NheI linearization. RNA was transcribed as above using the doubly purified DNA. The DNA and RNA were run on gels to ensure that the DNA and RNA encoded dimers.

Electrophysiology

Single-channel recordings were made from inside-out patches 1–6 days after RNA injection using an Axopatch 200A integrating patch clamp amplifier (Axon Instruments, USA). The recordings were done with symmetrical 67 mM KCl, 30 mM NaCl, 10 mM HEPES, 10 mM EGTA, and 1 mM EDTA (pH 7.2) for divalent cation-free recordings. Na-cGMP was included in the intracellular solution by isoosmolar replacement of NaCl. The acquired data was stored on VHS tape via a VR10B Digital Data Recorder (Instrutech Corp., USA) to a Sony-SLV400 VCR (Sony, Japan). Data were digitized at 20 kHz using a TL-1 DMA Interface and Pclamp 5.5 and 6.0 (Axon Instruments, USA) running on a Pentium-100mhz PC following low-pass filtering at 4 kHz (8 pole Bessel filter, Frequency Devices 902).

Data Analysis

The single-channel recordings were analyzed by the accumulation of data points into amplitude histograms in a program written in AXOBASIC (Axon Instruments, USA). For single-channel conductance, 5–10 s of recordings at +80 mV were made and openings were accumulated into an amplitude histogram. The histogram was fitted with two Gaussian functions with one Gaussian representing the closed state and one representing the main conducting open state. The difference between the mean of the open state Gaussian and mean of the closed state Gaussian is used to determine single-channel conductance. The amount of baseline included in these histograms is arbitrarily set; hence, the areas of the open state and closed state Gaussians do not reflect the P_O.

For open probabilities, 10–40 s of continuous recording in the presence of a specified concentration of cGMP at −80 mV was accumulated into an all-points amplitude histogram. The histograms were then fitted with up to four Gaussian functions, with one representing the closed state and the other three representing the three open states of the channel: the unprotonated, singly protonated, and doubly protonated subconductance states. As these histograms include all open and closed events, the area under the closed peak represents the closed probability (P_{closed}), and hence, the open probability (P_O) is equal to $1 - P_{closed}$. When the P_O is below 0.05, fitting Gaussians to the open states was difficult, and another approach was used where the Gaussian function fit to the closed state peak is first subtracted from the raw data. The portion of the resulting histogram corresponding to channel openings was defined by visual inspection, and the area underneath this region was calculated to obtain the number of points when the channels were open. This area was then divided by the entire area of the original histogram (total number of points) to yield the open probability (P_O).

To minimize any effects of spontaneous increases in apparent ligand affinity in cell-free patches (Gordon et al., 1992; Molokanova et al., 1997), dose response curves were measured using the following protocol. A series of decreasing concentrations of cGMP, ranging from 30 mM to 30 μM, was applied first, followed by the same set of cGMP solutions applied in order of increasing concentration. The P_O values at each concentration were determined and then averaged. Data were fit, using a nonlinear least squares routine, by the Hill equation: $P_O = P_{max}/[1 + (K_{1/2}/[A])^n]$, where [A] is the agonist concentration, and n is the Hill coefficient (with points weighted by $1/P_O$ for fits to individual channels or by the reciprocal of the standard deviation of each point for fits to mean dose response curves). Data are given as mean ± SEM (except for those cases in which n = 2 when given as mean ± range).

Theory

The three gating schemes considered in this study are shown in Figure 8. In all three schemes, we assume that the subunits of the channel undergo an activation gating reaction between a resting state and an active state. In accord with the nomenclature of Monod et al. (1965), we define the resting state as the "tense" (T) state and the active state as the "relaxed" (R) state. Since the channels function as homotetramers, we also have assumed that each subunit binds ligand in an identical and independent manner. The three schemes differ, however, in how the individual subunits interact to cause a channel to open.

Independent Subunit Model

In the independent subunit model (Figure 8A), each subunit undergoes an independent, allosteric transition between the resting T state (squares) and the active R state (circles). The allosteric equilibrium constant of this transition in the absence of ligand is thus defined as $L_0 = [T]/[R]$. The dissociation constants for binding of ligand to the resting T state and active R state of a subunit are K_T and K_R, respectively. The opening equilibrium constant for a subunit with ligand bound is given by $L_0 \cdot f$, where $f = K_R/K_T$. The probability that a subunit with bound agonist is in the active state, m_A, is then given by $m_A = 1/(1 + L_0 \cdot f)$, whereas the probability that a subunit without agonist bound is in the active state, m_0, is given by $m_0 = 1/(1 + L_0)$.

Since the channel is composed of four identical subunits, the full activation scheme of the channel is comprised of four independent, parallel reactions identical to that shown in Figure 8A. Figure 8D illustrates these four independent transitions for the spontaneous opening reaction of a channel in the absence of ligand. If we further assume that a channel is only open when all four of its subunits have activated, then this model becomes similar to a Hodgkin-Huxley scheme for a channel with four independent activation gates. The probability that a channel is spontaneously open in the absence of ligand, P_{sp}, is then given by $P_{sp} = m_0^4$, and the maximal probability that a channel is open at saturating ligand concentration, P_{max}, for a channel with four functional binding sites is then given by: $P_{max}(4) = m_A^4$. In general, for a channel with j functional binding sites, we have $P_{max}(j) = m_0^{(4-j)} \cdot m_A^j$.

A modification of the independent subunit model, proposed by Varnum and Zagotta (1995) has also been considered. In such schemes, the channels are allowed to open when only n out of the 4 subunits have activated, where n can equal 1, 2, or 3.

The maximal open probability at saturating ligand concentration for wild-type homomultimeric channels with 4 functional binding sites in which only n out of the 4 sites must activate, $P_{max}(n \mid 4)$, is given by:

$$P_{max}(n|4) = \sum_{j=n}^{4} \frac{4!}{(4-j)!j!} m_A^j (1 - m_A)^{(4-j)}$$

The spontaneous open probability in the absence of ligand is similarly:

$$P_{sp}(n|4) = \sum_{j=n}^{4} \frac{4!}{(4-j)!j!} m_0^{j} (1 - m_0)^{(4-j)}$$

Based on our experimental measurements of P_{max} and P_{sp}, we can solve the above two equations to obtain values for m_A and m_0 and hence obtain values for L_0 and f, for any given value of n. The maximal open probability at saturating ligand concentration for heteromultimeric channels containing k functional binding sites and (4 − k) nonfunctional sites, $P_{max}(n \mid k)$, is a complicated expression since for any given stoichiometry of wild-type and mutant subunits there are several possible combinations by which n subunits can activate. However, since m_A is very close to 1 (since P_{max} in wild-type channels is close to 1) whereas m_0 is close to 0 (since P_{sp} is very small), we can ignore most of these combinations and obtain the following approximate relations. When k = 3: $P_{max} \approx m_A^3(1 - m_0)$, regardless of whether n = 1, 2, or 3. When k = 2: $P_{max} \approx m_A^2(1 - m_0)^2$, when n = 1 or 2; $P_{max} \approx 2 \cdot m_A^2 m_0 \cdot (1 - m_0)$, when n = 3. When k = 1: $P_{max} \approx m_A(1 - m_0)^3$ for n = 1; $P_{max} \approx m_A m_0 \cdot (1 - m_0)^2$ for n = 2; and $P_{max} \approx 3 \cdot m_A m_0 \cdot (1 - m_0)^2$, when n = 3. (Note: m_A and m_0 are determined separately for each value of n, based on the above equations and our measurements of P_{sp} and P_{max} for wild-type channels. Thus, the calculated P_{max} values for each value of n will differ).

MWC Model

In the allosteric model of Monod, Wyman, and Changeux (Figure 8B), all four subunits of a channel undergo the transition between the resting T state and active R state in a single concerted conformational change as the channel opens. In this model, L_0 is the allosteric equilibrium constant for this opening transition in the absence of agonist. Thus, $P_{sp} = 1/(1 + L_0)$. Each agonist binding event stabilizes the channel in the open state by a factor of $f = K_R/K_T$, thereby shifting the equilibrium from the closed state to the open state by the term f^n, with n being the number of agonists bound to the channel. In terms of the scheme shown in Figure 8D, the MWC model, in the absence of agonist, reduces to the two extreme outside states. The opening equilibrium at saturating ligand concentration with four ligands bound is equal to $L_0 \cdot f^4$, and the maximal open probability is given by $P_{max}(4) = 1/[1 + L_0 \cdot f^4]$.

For channels with reduced numbers of ligand binding sites, j, we can write for saturating ligand concentrations: $P_{max}(j) = 1/[1 + L_0 \cdot f^j]$.

Coupled-Dimer Model

The coupled-dimer model (Figure 8C) represents a hybrid of the MWC and independent models. According to this model, the four subunits of a channel function as two independent dimers. Within a dimer, the two subunits undergo a concerted, MWC-like transition between a resting T state and an active R state. Each dimer, however, activates independently of the other dimer, and a channel is only open when both dimers enter the active R state. The ligand-independent states of the coupled dimer model consist of the two states of the MWC model and one intermediate state corresponding to a channel with one dimer in the active R state and one dimer in the resting T state (shaded symbols in Figure 8D). For each dimer, L_0 represents the agonist-independent equilibrium between the resting T state and active R state, and $L_0 f^n$ represents the equilibrium when a dimer has n ligands bound (where n can be 0, 1, or 2). According to this model, $P_{sp} = \{1/(1 + L_0)\}^2$ and $P_{max}(4) = 1/[1 + L_0 \cdot f^2]^2$.

The maximal open probability, $P_{max}(j)$, for channels with j functional binding sites is given by: $P_{max}(j) = (1/(1 + [L_0 f^n])) \cdot (1/(1 + [f^{(j-n)} L_0]))$, where n and j − n are the number of functional binding sites in each of the two dimers.

The independent, MWC, and coupled dimer models all permit us to solve directly for $P_{max}(j)$ based on measurements of P_{max} and P_{sp} for wild-type homomeric channels. For RO133 homotetramers, $P_{sp} = 1.25 \times 10^{-4}$ and $P_{max} = 0.95$ (Tibbs et al., 1997, 1998). From the above relations, we obtain the following values for L_0 and K_R/K_T: independent model in which all four subunits must activate, 9 and 1.4×10^{-3}; MWC model, 7999 and 5.1×10^{-2}; coupled dimer model, 99 and 1.6×10^{-2}. From these values and the above equations, we can then solve for the predicted values of the maximum open probability at saturating ligand concentration for channels with reduced numbers of ligand-binding sites, $P_{max}(j)$, for the three models. These predictions are illustrated in Figure 7.

MWC Model with Two Binding Constants

The MWC model was used to approximate how mutant subunits with some residual ability to bind ligand (such as RET/E) can be expected to contribute to channel activation. K_{R1} and K_{T1} are the dissociation constants for ligand binding to wild-type binding domains, and K_{R2} and K_{T2} are the dissociation constants for ligand binding to mutant binding domains. From fitting macroscopic dose reponse curves for wild-type homomeric channels with the MWC model, we obtain: $K_{R1} = 2$ μM and $K_{T1} = 39$ μM (Tibbs et al., 1998). Assuming that RET/E has a 2000-fold decreased affinity for cGMP, we obtain: $K_{R2} = 4000$ μM and $K_{T2} = 78{,}000$ μM. The following definitions were also used: $\alpha 1 = K_{R1}/[A]$, $\alpha 2 = K_{R2}/[A]$, $\beta 1 = K_{T1}/[A]$, $\beta 2 = K_{T2}/[A]$, $f_1 = (K_{R1}/K_{T1})$, and $f_2 = (K_{R2}/K_{T2})$, where [A] is the agonist concentration. Since there will be in general several open and closed states of the channel at any given cyclic nucleotide concentration, reflecting open and closed channels with 0–4 agonists bound, the probability that a channel will be open is given by $P_O = \Sigma[\text{open}]/(\Sigma[\text{open}] + \Sigma[\text{closed}])$, where $\Sigma[\text{open}]$ equals the sum of the probabilities of all possible open states, and $\Sigma[\text{closed}]$ equals the sum of the probabilities of all possible closed states.

For channels composed of three mutant subunits and one wild-type subunit, we obtain P_O from the following relations: $\Sigma[\text{open}] = (1 + 3 \cdot \alpha_2 + 3 \cdot \alpha_2^2 + \alpha_2^3 + \alpha_1 \cdot \alpha_2^3)$, and $\Sigma[\text{closed}] = L_0 \cdot f_1 \cdot f_2^3 \cdot (1 + 3 \cdot \beta_2 + 3 \cdot \beta_2^2 + \beta_2^3 + \beta_1 \cdot \beta_2^3)$.

For channels composed of two mutant subunits and two wild-type subunits, we obtain: $\Sigma[\text{open}] = (1 + 2 \cdot \alpha_2 + \alpha_2^2 + 2 \cdot \alpha_1 \cdot \alpha_2^2 + \alpha_1^2 \cdot \alpha_2^2)$, and $\Sigma[\text{closed}] = L_0 \cdot f_1^2 \cdot f_2^2 \cdot (1 + 2 \cdot \beta_2 + \beta_2^2 + 2 \cdot \beta_1 \cdot \beta_2^2 + \beta_1^2 \cdot \beta_2^2)$.

For channels containing one mutant subunit and three wild-type subunits, we obtain: $\Sigma[\text{open}] = (1 + \alpha_2 + 3 \cdot \alpha_1 \alpha_2 + 3\alpha_1^2 \alpha_2 + \alpha_1^3 \alpha_2)$, and $\Sigma[\text{closed}] = L_0 \cdot f_1^3 \cdot f_2 \cdot (1 + \beta_2 + 3\beta_1 \beta_2 + 3\beta_1^2 \beta_2 + \beta_1^3 \beta_2)$.

Acknowledgments

We thank Arthur Karlin, Jian Yang, and Edgar Young for helpful comments on the manuscript, and Huan Yao and John Riley for technical assistance.

Received April 1, 1998; revised May 18, 1998.

References

Altenhofen, W., Ludwig, J., Eismann, E., Kraus, W., Boenigk, W., and Kaupp, U.B. (1991). Control of ligand specificity in cyclic nucleotide-gated channels from rod photorepectors and olfactory epithelium. Proc. Natl. Acad. Sci. USA *88*, 9868–9872.

Bucossi, G., Nizzari, M., and Torre, V. (1997). Single-channel properties of ionic channels gated by cyclic nucleotides. Biophys. J. *72*, 1165–1181.

Czajkowski, C., and Karlin, A. (1991). Agonist binding site of *Torpedo* electric tissue nicotinic acetylcholine receptor: a negatively charged region of the δ subunit within 0.9nm of the α subunit binding site disulfide. J. Biol. Chem. *266*, 22603–22612.

Finn, J.T., Grunwald, M.E., and Yau, K.-W. (1996). Cyclic nucleotide-gated ion channels: an extended family with diverse functions. Annu. Rev. Physiol. *58*, 395–426.

Gordon, S.E., and Zagotta, W.N. (1995a). A histidine residue associated with the gate of the cyclic nucleotide-activated channels in rod photoreceptors. Neuron *14*, 177–183.

Gordon, S.E., and Zagotta, W.N. (1995b). Subunit interactions in coordination of Ni^{2+} in cyclic nucleotide-gated channels. Proc. Natl. Acad. Sci. USA *92*, 10222–10226.

Gordon, S.E., Brautigan, D.L., and Zimmerman, A.L. (1992). Protein phosphatases modulate the apparent agonist affinity of the light-regulated ion channel in retinal rods. Neuron *9*, 739–748.

Goulding, E.H., Ngai, J., Kramer, R.H., Colicos, S., Axel, R., Siegelbaum, S.A., and Chess, A. (1992). Molecular cloning and single-channel properties of the cyclic nucleotide-gated channel from catfish olfactory neurons. Neuron *8*, 45–58.

Goulding, E.H., Tibbs, G.R., Liu, D., and Siegelbaum, S.A. (1993). Role of H5 domain in determining pore diameter and ion permeation through cyclic nucleotide-gated channels. Nature *364*, 61–64.

Goulding, E.H., Tibbs, G.R., and Siegelbaum, S.A. (1994). Molecular mechanism of cyclic-nucleotide-gated channel activation. Nature *372*, 369–374.

Hodgkin, A.L., and Huxley, A.F. (1952). A quantitative description of membrane current and its application to conduction and excitation in nerve. J. Physiol. (Lond.) *117*, 500–544.

Ildefonse, M., and Bennett, N. (1991). Single-channel study of the cGMP-dependent conductance of retinal rods from incorporation of native vesicles into planar lipid bilayers. J. Membr. Biol. *123*, 133–147.

Jackson, M.B. (1989). Perfection of a synaptic receptor: kinetics and energetics of the acetylcholine receptor. Proc. Natl. Acad. Sci. USA *86*, 2199–2203.

Kaupp, U.B., Niidome, T., Tanabe, T., Terada, S., Boenigk, W., Stuehmer, W., Cook, N.J., Kangawa, K., Matsuo, H., Hirose, T., et al. (1989). Primary structure and functional expression from complementary DNA of the rod photoreceptor cyclic GMP-gated channel. Nature *342*, 762–766.

Ketchum, K.A., Joiner, W.J., Sellers, A.J., Kaczmarek, L.K., and Goldstein, S.A. (1995). A new family of outwardly rectifying potassium channel proteins with two pore domains in tandem. Nature *376*, 690–695.

Li, J., Zagotta, W.N., and Lester, H.A. (1997). Cyclic nucleotide-gated channels: structural basis of ligand efficacy and allosteric modulation. Q. Rev. Biophys. *30*, 177–193.

Liman, E.R., Tytgat, J., and Hess, P. (1992). Subunit stoichiometry of a mammalian K^+ channel determined by construction of multimeric cDNAs. Neuron *9*, 861–871.

Liu, D.T., Tibbs, G.R., and Siegelbaum, S.A. (1996). Subunit stoichiometry of cyclic nucleotide-gated channels and effects of subunit order on channel function. Neuron *16*, 983–990.

Ludewig, U., Pusch, M., and Jentsch, T.J. (1996). Two physically distinct pores in the dimeric ClC-0 chloride channel. Nature *383*, 340–343.

MacKinnon, R. (1991). Determination of the subunit stoichiometry of a voltage-activated potassium channel. Nature *350*, 232–235.

McCormack, K., Joiner, W.J., and Heinemann, S.H. (1994). A characterization of the activating structural rearrangements in voltage-dependent *Shaker* K^+ channels. Neuron *12*, 301–315.

Middleton, R.E., Pheasant, D.J., and Miller, C. (1996). Homodimeric architecture of a ClC-type chloride ion channel. Nature *383*, 337–340.

Molokanova, E., Trivedi, B., Savchenko, A., and Kramer, R.H. (1997). Modulation of rod photoreceptor cyclic nucleotide-gated channels by tyrosine phosphorylation. J. Neurosci. *17*, 9068–9076.

Monod, J., Wyman, J., and Changeux, J.P. (1965). On the nature of allosteric transitions: a plausible model. J. Mol. Biol. *12*, 88–118.

Perutz, M.F., Fermi, G., Luisi, B., Shaanan, B., and Liddington, R.C. (1987). Stereochemistry of cooperative mechanisms in hemoglobin. Acc. Chem. Res. *20*, 309–321.

Picones, A., and Korenbrot, J.I. (1995). Spontaneous, ligand-independent activity of the cGMP-gated ion channels in cone photoreceptors of fish. J. Physiol. (Lond.) *485*, 699–714.

Root, M.J., and MacKinnon, R. (1994). Two identical noninteracting sites in an ion channel revealed by proton transfer. Science *265*, 1852–1856.

Royer, W.E., Heard, K.S., Harrington, D.J., and Chiancone, E. (1995). The 2.0 Å crystal structure of Scapharca tetrameric hemoglobin: cooperative dimers within an allosteric tetramer. J. Mol. Biol. *253*, 168–186.

Ruiz, M., and Karpen, J.W. (1997). Single cyclic nucleotide-gated channels locked in different ligand-bound states. Nature *389*, 389–392.

Schoppa, N.E., McCormack, K., Tanouye, M.A., and Sigworth, F.J. (1992). The size of gating charge in wild-type and mutant *Shaker* potassium channels. Science *255*, 1712–1715.

Shabb, J.B., and Corbin, J.D. (1992). Cyclic nucleotide-binding domains in proteins having diverse functions. J. Biol. Chem. *267*, 5723–5726.

Stryer, L. (1987). Visual transduction: design and recurring motifs. Chemica Scripta, *27B*, 161–171.

Taylor, W.R., and Baylor, D.A. (1995). Conductance and kinetics of single cGMP-activated channels in salamander rod outer segments. J. Physiol. (Lond.) *483*, 567–582.

Tibbs, G.R., Goulding, E.H., and Siegelbaum, S.A. (1997). Allosteric activation and tuning of ligand efficacy in cyclic-nucleotide-gated channels. Nature *386*, 612–615.

Tibbs, G.R., Liu, D.T., Leypold, B.G., and Siegelbaum, S.A. (1998). A state-independent interaction between ligand and a conserved arginine residue in cyclic nucleotide-gated channels reveals a functional polarity of the cyclic nucleotide binding site. J. Biol. Chem. *273*, 4497–4505.

Tytgat, J., and Hess, P. (1992). Evidence for cooperative interactions in potassium channel gating. Nature *359*, 420–423.

Varnum, M.D., and Zagotta, W.N. (1996). Subunit interactions in the activation of cyclic nucleotide-gated ion channels. Biophys. J. *70*, 2667–2679.

Varnum, M.D., Black, K.D., and Zagotta, W.N. (1995). Molecular mechanism for ligand discrimination of cyclic nucleotide-gated channels. Neuron *15*, 619–625.

Weber, I.T., and Steitz, T.A. (1987). Structure of a complex of catabolite gene activator protein and cyclic AMP refined at 2.5 Å resolution. J. Mol. Biol. *198*, 311–326.

Zagotta, W.N., and Siegelbaum, S.A. (1996). Structure and function of cyclic nucleotide-gated channels. Annu. Rev. Neurosci. *19*, 235–263.